SoundBender: Dynamic Acoustic Control Behind Obstacles

Mohd Adili Norasikin, Diego Martinez Plasencia, Spyros Polychronopoulos, Gianluca Memoli, Yutaka Tokuda, Sriram Subramanian
School of Engineering and Informatics, University of Sussex, Brighton, United Kingdom
{m.norasikin, dm372, s.polychronopoulos, g.memoli, y.tokuda, sriram}@sussex.ac.uk

ABSTRACT
Ultrasound manipulation is growing in popularity in the HCI community with applications in haptics, on-body interaction, and levitation-based displays. Most of these applications share two key limitations: a) the complexity of the sound fields that can be produced is limited by the physical size of the transducers; and b) no obstacles can be present between the transducers and the control point. We present SoundBender, a hybrid system that overcomes these limitations by combining the versatility of phased arrays of transducers (PATs) with the precision of acoustic metamaterials. In this paper, we explain our approach to design and implement such hybrid modulators (i.e. to create complex sound fields) and methods to manipulate the field dynamically (i.e. stretch, steer). We demonstrate our concept using self-bending beams enabling both levitation and tactile feedback around an obstacle and present example applications enabled by SoundBender.

Author Keywords
Acoustic manipulation; Metamaterials; Self-bending beams.

INTRODUCTION
The idea to control matter at a distance to create user interfaces has fuelled HCI research, from the inception of the Ultimate display [1], to Ishi's vision, Radical Atoms [2].

Various approaches for contactless manipulation of matter in mid-air have been explored, exploiting aerodynamics [3] or magnetophoresis [4]. The use of ultrasound [5–7] has received particular attention compared to other contactless manipulation approaches, for two essential reasons. First, by using non-audible sound waves, the approach provides its affordances (i.e. levitation, tactile feedback) without interfering with audio modalities (e.g. no parasitic noise). Second, ultrasound manipulation only depends on the acoustic pressure of the sound field and, in the case of levitation, on the object's density. No other physical properties (e.g. magnetic, electric) are required, allowing acoustic levitation to be applied to materials ranging from polystyrene beads to coloured liquid [8], or even food [9].

UIST '18, October 14–17, 2018, Berlin, Germany

ACM ISBN 978-1-4503-5948-1/18/10…$15.00
https://doi.org/10.1145/3242587.3242590

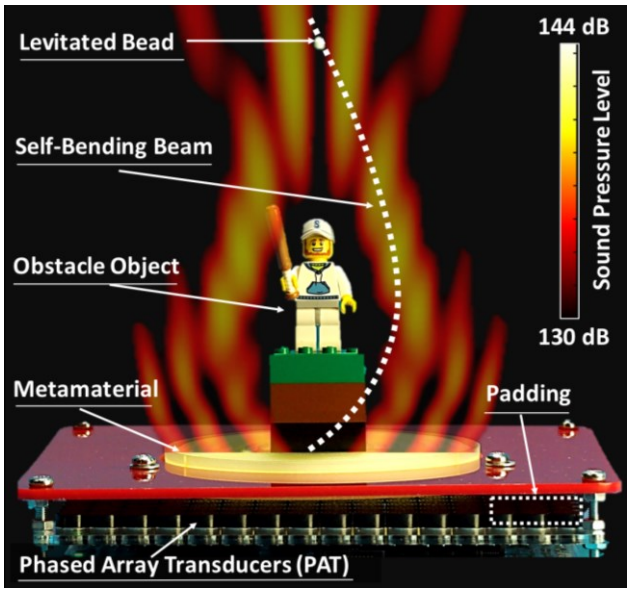

Figure 1. SoundBender combines ultrasound transducer arrays and acoustic metamaterials to create self-bending beams. The self-bending beam allows for dynamic features (e.g. levitation) above passive props, while the phased array allows interactive 3D control of the position of the feature.

Most previous approaches of ultrasound manipulation rely on the use of arrays of ultrasonic transducers, either to create standing waves [10,11] or more complicated fields, like multi-point feedback [12] or acoustic tweezers [7].

However, the physical size of the transducers limits the resolution of the sound fields that can be created. According to the Nyquist theorem, reconstructing a sound field of a specific frequency will require the sound sources to be separated less than half of the wavelength of that frequency (modulator pitch less than $\lambda/2$). However, the size of commercially available ultrasound transducers easily exceeds this threshold (e.g. at 40 kHz; $\lambda/2 \approx 4.3$ mm).

Acoustic metamaterials allow for a much smaller modulator pitch, avoiding this limitation. Acoustic metamaterials are assemblies of unit cells, each inducing a local change in the phase and/or intensity of the incoming acoustic waves. Since metamaterials can be easily 3D printed, the size of

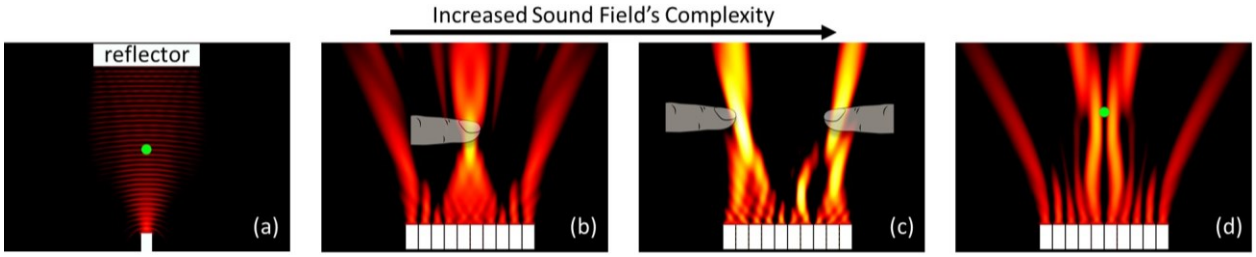

Figure 2. Example sound fields of increased complexity, created using PATs: (a) Standing wave (using a transducer and a reflector); (b) single focal point; (c) multiple focal points; and (d) tweezer trap for one sided levitation.

each cell can be designed to offer the required modulator pitch (i.e. cell size < λ/2), even in the ultrasonic frequency range. These have been applied to control vibrations [14] and sound [15,16]. As a main benefit, acoustic metamaterials can encode complex fields. However, they are usually static in nature (do not change over time). Also, their use to create interactive features remains unexplored.

In this paper, we present SoundBender, a hybrid ultrasound modulator, combining the benefits of acoustic metamaterials and phased arrays of transducers (PATs). The metamaterial encodes a complex but static sound field (e.g. an acoustic hologram), while the PAT adds dynamic and real-time control (e.g., move /stretch the sound field in 3D, swap between levitation and tactile functionalities).

Our contribution is two-fold: First, we provide a method to exploit the potential of hybrid modulators combining PAT and metamaterials. Second, we illustrate this method for the case of dynamic self-bending beams. These allow the sound field to bend around objects placed on top of the modulator and create interactive features (e.g. levitating objects, tactile points) which can be manipulated in 3D above the passive prop using the PAT (see Figure 1). We validate our contributions by evaluating the ability of our approach to recreate the intended sound fields (self-bending beams) and dynamically control them, and finalize the paper by discussing example application scenarios and further potential of SoundBender for the HCI community.

RELATED WORK

We propose a hybrid approach, combining a PAT and acoustic metamaterials. In this section, we review relevant literature in these areas, identifying their strengths, limitations and the key techniques SoundBender leverages to combine these approaches and create such hybrid modulators.

Transducer-based sound manipulation

Acoustic levitation was firstly observed more than 150 years ago, with small dust particles being trapped in the low-pressure lobes of a standing wave [17] (as in Figure 2a). This inspired the first example of particle levitation using a transducer and an opposing reflector plate [18].

This approach, using either a transducer and reflector or a pair of opposing transducers, has later been extensively used within the HCI community. PixieDust [5] used two pairs of opposing PATs to create floating visualizations. It exploited the repeated lobe pattern within standing waves to levitate composite shapes. It also shifted the phase of the transducers to move these shapes in 3D. LeviPath [6] allowed the 3D displacements of single particles, but constrained to specific directions. JOLED [10] presented a game based on levitated voxels, where the rotation of the levitated object was controlled using electrostatic charge.

The examples above only allow for the shifting of a fixed sound field and require paired arrangements. Other approaches exploit sound interference to achieve more control over the sound field (and one-sided setups). Carter et al. [19] used constructive interference at a focal point (see Figure 2b). Modulating the ultrasound wave at 200Hz allowed skin receptors to perceive acoustic radiation, enabling mid-air tactile sensations. Long et al. [12] extended this method for multi-point arrangements (see Figure 2c). Drawing inspiration from holographic methods, Marzo et al. [20] achieved further control on the complexity of the sound field. They demonstrate one sided acoustic control and implement several manipulation tools, such as tweezers (see Figure 2d) or other types of levitation traps, such as those used in Floating Charts [21] for data visualization. Levitate [11] introduced path tracing algorithms to animate multiple voxels in 3D space. These approaches have also been used for tools [22] or gloves [7].

These solutions rely on PATs, which offers excellent control in terms of phase and amplitude. However, the size of existing ultrasound transducers limits the minimum pitch possible for a PAT modulator (i.e., separation between its sources/transducers). This minimum pitch limits the maximum frequency of the fields a PAT can generate.

As introduced earlier, sources must be separated less than $\lambda/2 \approx 4.3$ mm, to recreate a sound field at 40kHz (Nyquist). Let's consider a PAT of 16x16 transducers, each of size 10mm (e.g. Ultrahaptics, version 2.0.0, pitch 10mm). From an FFT analysis, the maximum temporal frequency that can be reconstructed by this discrete set of sources is ~15kHz [13]. This does not mean they cannot reproduce any sound field at 40kHz, but it limits their application to sound fields with a higher spatial resolution.

A similar 16x16 setup, but with sources spaced $\lambda/2$, would allow reconstruction at ~35kHz. A higher number of sources can marginally increase these limits, but only a pitch less than $\lambda/2$ will allow reconstruction at full 40kHz.

	Field control	Spatial resolution	Obstacle Avoidance
Transducer Pair [5,18]	Dynamic (reduced)	Low	N/A
Transducer Array [6,12,21]	Dynamic	Low	N/A
Metamaterial [30,45]	Static	High	Static
Hybrid Approach (SoundBender)	Dynamic	High	Dynamic

Table 1. Related approaches and relevant features.

Thus, the limiting factor for PATs is the size of its transducers. Transducers require a parabolic plate, to help direct and focus the acoustic pressure. However, the size of the radiating area (D) of the parabolic plate must be kept larger than λ ($D >> \lambda$) [23]. This practically limits the minimum size of focused transducers (and the minimum pitch of a PAT) to be larger than λ. Non-focused, flat mounted transducers [24] allow smaller sizes (~6mm, still larger than $\lambda/2$). Their lower radiating pressure also make them unsuitable for HCI usage, such as for levitation [23].

Acoustic Metamaterials

Research in physics has explored a variety of acoustic metamaterials to achieve more precise sound field control beyond the transducers' limits. Acoustic metamaterials are elements specially designed to adjust the phase and amplitude of the incoming wave and manipulate the sound field (e.g. direct the focal point). These have been successfully used to create negative diffraction [25], self-bending beams [26], acoustic holograms [27], 2D letters made of sound [28], structures to deviate seismic waves [29] and also acoustic levitation [30]. Metamaterials can be easily 3D printed and provide sound fields with higher spatial resolution than transducers alone can provide[25].

Memoli et al. [30] recently explored the use of metamaterials in the ultrasound region (40 kHz). More interestingly, they demonstrated that sound fields with high spatial resolution can be created from a discrete set of only 16 "phase-delay bricks", with a constant amplitude. This indicates that a small modulator pitch (high density of sources) is more significant than phase or amplitude resolution in order to create a sound field with precision.

These findings highlight the strengths of metamaterials (modulator pitch less than $\lambda/2$) over PATs (accurate phase/amplitude control, but higher distance between sources). SoundBender draws on these findings to propose our hybrid approach. Besides, the possibility to discretize sound fields with a small set of 16 bricks facilitates fabrication, a feature that we exploit later in the paper.

As a main drawback, metamaterials are in most cases static. Thus, they are tailored to one specific function, but miss the dynamic control of phase and amplitude that the PAT can provide. Some designs use moving parts [31,32], but still only allow minor changes in the sound field created. SoundBender overcomes this, by delegating the dynamic control to the phased array and using HOE approaches [33, 34] to control the field (e.g. stretching, steering, etc.).

Self-bending beams

The concept of self-bending beams (used in this paper to illustrate our approach) was initially used in engineering applications, to obscure buildings from noise [35] or protect areas from earthquakes [29]. Such beams can produce a focal point at the end of the curve [36,37] and act as single beam acoustic tweezers [38–40]. With the abilities of obscuring obstacles and self-healing [36,37,41,42], self-bending beams show a promising method to allow obstacle avoidance [43,44], which has limited other levitation/haptics approaches (e.g. occlusions due to hands).

The first practical realization of self-bending in acoustics [41] utilized PATs emitting audible sound (10kHz; $\lambda \approx 34.4$ mm). This allowed using commercial 16 mm transducers (i.e. smaller than $\lambda/2$), but made it inappropriate for HCI purposes (i.e. it produced an audible constant high pitch sound at 10kHz). Li et al. [26] implemented self-bending beams using metamaterials, but still limited to the audible frequency range (3.4 kHz). Norasikin et al. [45] presented the first implementation in the ultrasound region (40kHz) and achieved levitation of objects larger than $\lambda/2$.

SoundBender extends these previous approaches as shown in Table 1. It uses a hybrid approach (combine a static metamaterial and a PAT) to allow: **i)** the creation of either levitation or tactile points beyond occluding objects; **ii)** the dynamic 3D manipulation of the sound field (use the phased array to move the points); and **iii)** a structured method to create such hybrid modulators.

SOUNDBENDER: HYBRID SOUND MODULATORS AND DYNAMIC SELF-BENDING BEAMS

In this work, we present SoundBender (illustrated in Figure 1): a hybrid modulator combining acoustic metamaterials and a PAT. The metamaterial provides a low modulator pitch, key to create sound fields with high spatial resolution (but static). The PAT adds dynamic amplitude/phase control of the field (at lower resolution).

As one of our main contributions, we describe a method to implement such hybrid modulators, drawing on acoustics and metamaterial techniques. The following subsections describe the main stages within our method: **i)** computation of the self-bending curve; **ii)** computation of the transducers' phases to recreate the sound field; **iii)** discretization into 3D printable bricks and fabrication of the metamaterial; **iv)** Modulators spacing and coupling; and **v)** the PAT: algorithms for dynamic control. The following subsections detail each of these five steps.

Please note that we illustrate our approach by encoding a self-bending beam into the metamaterial. This allows us to place passive props (e.g. decorative features, toys) on top of our modulators, and still create dynamic control points (e.g.

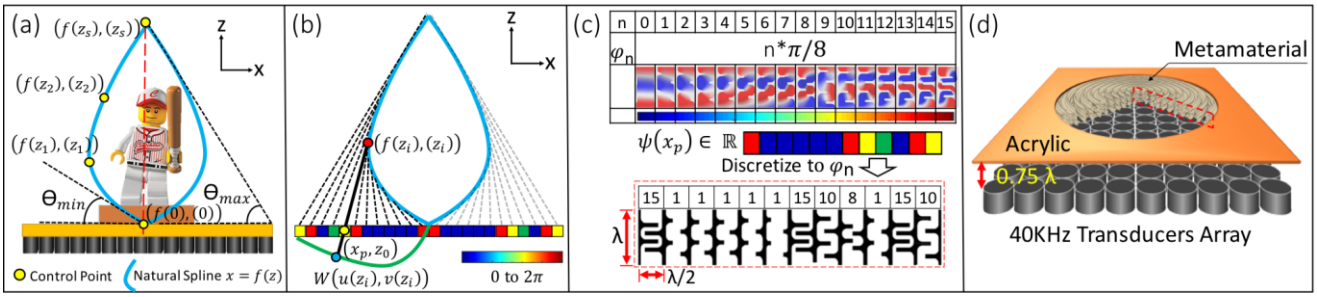

Figure 3. Summary of method (a) We identify a few points around the prop and compute a curve/spline;(b) we compute the phases producing a self-bending beam from this spline; (c) we discretize phases using a reduced set; (d) final metamaterial and setup.

movable levitation traps or tactile points) above the prop. The first two steps described next are specific for self-bending beams. However, the other steps in our method can be reused for other scenarios, and step **ii)** provides pointers to aid its application for other sound fields/examples.

i) Computation of the self-bending curve

The self-bending beam must wrap around the passive prop located on the metamaterial (see Figure 3a), to avoid disruption (energy scattering from the prop's surface and distorting the sound field). To do this, we compute a convex hull to fit the prop. Each point of the convex hull must be (at least) $\lambda/2 \cong 4.3mm$ away from the prop (due to the "thickness" of the beam itself). Further space must be allowed if the beam will be dynamically changed (e.g. move tactile/levitation points up/down or to the sides), using the control techniques described later in step **v)**.

We then use natural splines [46], to compute the desired curve ($x = f(z)$) from the S points on the convex hull ($f(z_i)$, z_i), as shown in Figure 3a. It must be noted that both the starting and end points must lie on the central axis of the material ($xy = 0$). The convex hull must avoid points lying less than θ_{min}=30 degrees from the horizontal plane (i.e. outside of the directivity pattern of our transducers). This θ_{min} is used as the orientation to clamp the starting point ($f(z_0)$, z_0) of the spline. The end point ($f(z_S)$, z_S) is clamped at an angle connecting the point to the last cell in the metamaterial (θ_{max}). Besides, the projection of the curve tangents on the metamaterial (black lines in Figure 3b) must be injective (two tangents cannot reach the same point x_p).

ii) Computation of phases to recreate the sound field

The steps above allow us to compute a spline path closely wrapping the object's shape. We simplified the approach by Zhang et al. [41] [1], to compute the phases that produce a self-bending beam following such path, and report these equations and method here. Our method will first compute the self-bending beam on a 2D plane (XZ), computing the phase delays of the sound sources along the axis X (see Figure 3b). Next, we revolve this 1D profile to compute the phases on our 2D metamaterial (see Figure 3d).

Let $x = f(z)$ be our spline path and let $\mathbf{P}(f(z),z)$ be points along this spline ($z \in [0, z_s]$). As per [41], for each spline point $\mathbf{P}(f(z),z)$ we compute a matching point $\mathbf{W}(u(z), v(z))$ on the wave-front producing a caustic tangent to our spline:

$$u(z) = \frac{I(z)}{\sqrt{1+f'(z)^2}} - \frac{f'(z)\left(f(z)-z\cdot f'(z)\right)}{1+f'(z)^2} \qquad (1)$$

$$v(z) = \frac{f'(z)\cdot I(z)}{\sqrt{1+f'(z)^2}} + \frac{f(z)-z\cdot f'(z)}{1+f'(z)^2}$$

$$I(z) = \int \frac{\left(f(z)-z\cdot f'(z)\right)f''(z)}{(1+f'(z)^2)^{\frac{3}{2}}}$$

We then project the caustic wave-front **W** (Figure 3b) onto our metamaterial plate. The points $\mathbf{W}(u(z), v(z))$ can then be projected to a position $x_p(z)$ with phase $\psi(x_p(z))$ as follows:

$$x_p(z) = v(z) + u(z)\cdot u'(z)/v'(z) \qquad (2)$$

$$\psi(x_p(z)) = (2\pi/\lambda)\cdot u(z)/\cos(\arctan(u'(z)/v'(z)))$$

Please note that each point of the curve $\mathbf{P}(f(z),z)$ will result in a position $x_p(z)$ and phase $\psi(x_p(z))$ along the X axis. This explains the need for the projected tangents to be injective (i.e. no two tangents projected to the same x_p).

The next step is to transform the current 1D profile (phases along axis X) into our 2D plane. We do this by revolving the profile along the Z axis, creating our enclosing self-bending volume. Thus, the phase for any point (x_p,y_p,0) on the metamaterial plate is computed as follows:

$$\psi(x_p, y_p) = \psi\left(\sqrt{{x_p}^2 + {y_p}^2}\right) \qquad (3)$$

The steps above are specific for the recreation of self-bending beams. Hybrid modulators could be created, with the metamaterial encoding other sound fields (e.g. a multipoint field as in [12]; or generic holographic approaches as in [47]). In any case, the next steps in our method can be reused with such other approaches, as long as the phase $\psi(x_p, y_p)$ for any point on the metamaterial surface is known.

[1] Our simplified equations are still equivalent to those in [41]. Simplification is possible as our first point is **P**(0,0), resulting in term $C(z_0)$ becoming zero. All derivatives are made relative to z, using chain rule. First order and second order derivatives (e.g. $f'(z)$ and $f''(z)$) can be numerically approximated easily, using central differences.

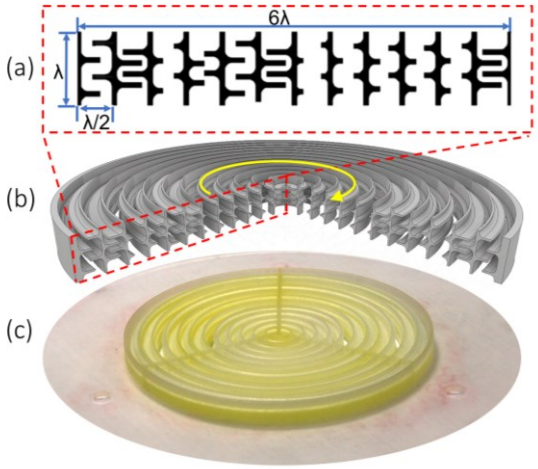

Figure 4. Metamaterial 3D Printing Model: (a) 2D drawing of encoded metamaterial bricks; (b) 3D Sliced view of metamaterial model after revolving the 2D drawing sketch; (c) Final 3D printed metamaterial (with support base).

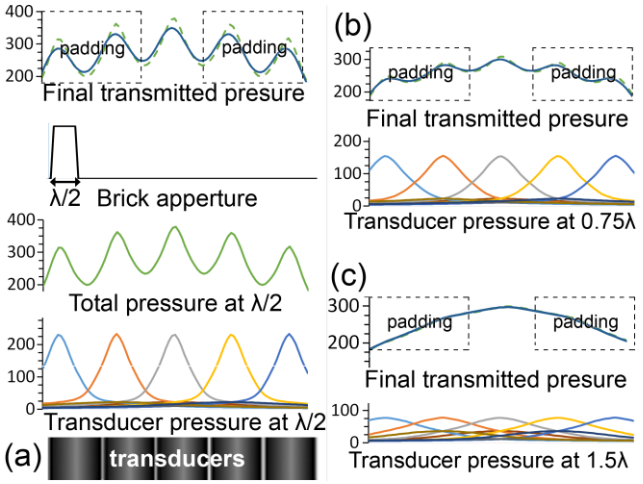

Figure 5. Effects of spacing between PAT and metamaterial. (a) Pressure transmitted through our bricks with a gap $\lambda/2$, considering directivity, attenuation and brick's aperture size. Comparison of pressure with gaps 0.75 λ (b) and 1.5 λ (c).

iii) Discretization and fabrication of the metamaterial

The phase distribution $\psi(x_p, y_p)$ above describes the phase required at each point $(x_p, y_p, 0)$ on the modulator's surface. We then discretize $\psi(x_p, y_p)$ using the set φ_{16} of 16 metamaterial bricks proposed by Memoli et al. [30], to encode the metamaterial. These bricks are optimized for high transmission at 40 kHz, and each one encodes a different phase delay (between 0 to 2π) as shown in Figure 3c. Such bricks have a thickness of λ, and lateral dimension (pitch) of $\lambda/2 \approx 4.3mm$, fitting our size requirements.

To discretize the continuous phase distribution $\psi(x_p, y_p)$, we sample the 2D plane with a separation of $\lambda/2$ (size of a brick), and round the phase to the closest value in the brick set φ_{16} (bricks and phase values visible in Figure 3c, top).

The above is a generic approach, applicable to any sound field distribution. For axisymmetric phase distributions (like our self-bending beams), a more accurate alternative it to encode the phase from the original 1D profile $\psi(x_p)$, by revolving it (red outline in Figure 3d) around the Z axis. This provides a continuous approximation to all points on the same ring, reducing discretization to the radial direction.

We did this as shown in Figure 4a. We encoded the metamaterial bricks without gaps and designed the 2D sketch. We revolved this sketch (see Figure 4b) using a 3D modelling software (Autodesk Inventor Professional 2017). Finally, we fabricated this 3D model using a high-precision 3D printer (ProJet HD 3000 Plus printer) and VisiJet® EX200 material (high tensile strength). Precision of the 3D printer is critical to reproduce the original phase distribution, as the size of the bricks is at the limit of Nyquist theorem (<4.3mm, in our case). High tensile strength ensures acoustic radiation is transmitted (and not absorbed) by the metamaterial. Figure 4c shows the final metamaterial, including a support base to ease assembly.

iv) Modulators spacing and coupling

A gap will exist between the metamaterial and the PAT, and the size of this gap will play affect the performance of the hybrid modulator, as we describe and analyse here.

A small gap will produce an uneven distribution of acoustic pressure across the metamaterial surface, being strong for bricks in front of a transducer, but weak for bricks between transducers. In contrast, a bigger gap will provide a more even distribution, but thickness of the modulator will increase (footprint), power will be lost (i.e. the sources are farther apart) and each brick will receive contribution from more transducers (i.e. the phase of a brick is not ruled by the phase of the closest transducer, but by a group of them). This last issue can affect the effectiveness of the dynamic control techniques described in the next section.

We analysed the effect of various gap sizes, as illustrated in Figure 5 (all pressure values relative to the transducer's pressure at 1m (p_{ref})). We first modelled the pressure distribution created by a section of 5x5 transducers at various distances above the PAT (from 0.5λ to 1.5λ). We considered directivity (extracted from [24]) and attenuation with distance, and computed total pressure distribution from our transducers at the target distance. We could not assume specific positions for the bricks in front of the transducers (size of a brick is not a multiple of the transducer size). Thus, we modelled the aperture of a brick as a rectangular function of size $\lambda/2$ x $\lambda/2$ (i.e. size of a brick), computing the pressure transmitted through the brick as the convolution of the signal and its aperture.

This analysis illustrates the tendencies introduced earlier. Figure 5a illustrates a gap of size $\lambda/2$ (minimum distance for the acoustic wave to be transferred as a plane wave). Pressure across bricks would vary unevenly, between 248 and 349 p_{ref} (13% coefficient of variation). This spacing, however, maximizes the coupling of the phases of the array

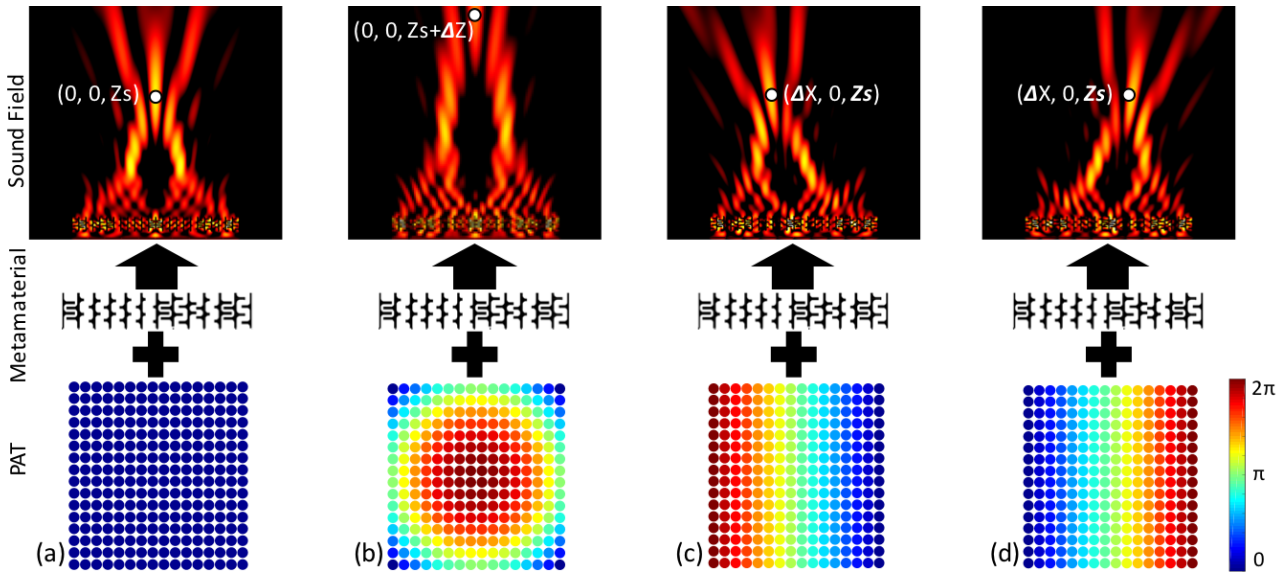

Figure 6. Using our control algorithm for several displacements (*Δx, Δy, Δz*): (a) No displacement; (b) Vertical displacement, (*Δz=1cm)*; (c) Steering left (*Δx=-1cm)*; (d) Steering right (*Δx=1cm).* Note All operators rely on smooth phase distributions.

to the metamaterial. In a best case scenario (brick in front of a transducer) 66% of the pressure will come from the closest transducer. In a worst case (brick in the gap between 4 transducers), 65% of the pressure will come from the four transducers (i.e. phase will receive contribution from the closest 2x2 transducers). A bigger gap of 1.5λ (Figure 5c) provides a more even distribution (282-297 p_{ref} ; ~1.6% variation). However only a 27% percent of pressure will come from the closest transducer (best case scenario) and only 58% from the closest 2x2 transducers (worst case).

Our analysis revealed that a gap of 0.75λ (Figure 5b) provides a good general solution to this trade-off. Amplitude variation across the plane remains homogeneous (265-300 p_{ref}; 4.5% variation). Amplitude contribution remains focussed, with 51% coming from only the closest transducer (best case scenario) and 68% from the closest 2x2 transducers (worst case, between transducers).

Relevant insight can be gained from this analysis, useful for designers exploring the use of hybrid modulators. First, the gradual change on the transducer's contribution to each brick shows that the gap will behave as a smoothing function, interpolating intermediate phase values from the lower resolution PAT. Such smoothing indicates that phase distributions on the PAT should only use low frequency distributions (i.e. sharp changes might be lost due to smoothing). While this is not an issue for the algorithms in step **(v)** (*diffraction* and *Fresnel lens* are low frequency functions), practitioners using control algorithms requiring higher frequencies will probably need to minimize this gap.

Second, a loss of power is observed in our pressure distributions in front of the two leftmost and rightmost transducers (see "padding" areas in Figure 5). These areas miss contribution from transducers further to the left and right. To avoid this, it is recommendable to use a PAT larger than the metamaterial plate, "padding it" with two extra rows of transducers. The central transducers receive minimal contribution from additional transducers. Thus, by padding with two extra transducers, our distributions can be assumed periodical for all the plate.

v) The PAT: Algorithms for dynamic control

The previous stages describe the creation of our hybrid modulator, but this alone would only allow the recreation of the static sound field encoded in the metamaterial. Here we describe techniques to control this field dynamically, by using our PAT. Two types of manipulations are enabled: **i)** global displacement of the field; and **ii)** switching between tactile feedback and levitation traps.

Global displacement of the sound field

We exploit a combination of a *diffraction grating* and a *Fresnel lens* algorithm, similar to those used in the control of holographic optical tweezers [33,34].

Let (i,j) be one of the transducers in our array, and $(x_i, y_j, 0)$ be its 3D position. Let $\mathbf{P}(0,0,z_s)$ be the reference point in our field (e.g. see top of the self-bending beam, in Figure 6a). Let $(\Delta x, \Delta y, \Delta z)$ be the displacement to apply to that point. Each transducer phase $\psi\,(i,j)$ is computed as follows:

$$\psi(i,j) = \underbrace{\frac{2\pi}{\lambda \cdot z_S}(x_i\,\Delta x + y_j\,\Delta y)}_{Diffraction\ grating} + \underbrace{\frac{\pi \cdot \Delta z}{\lambda \cdot {z_S}^2}({x_i}^2 + {y_j}^2)}_{Fresnel\ lens} \quad (4)$$

The manipulation above will displace the reference point (actually, any point on the plane $Z=z_s$) as described by $(\Delta x, \Delta y, \Delta z)$. While correct for planar fields like in [47], the *Fresnel lens* effect will make the sound field to be squashed or stretched (Figure 6b). The *diffraction grating* will cause a shearing effect (Figure 6c and 6d). Spline definition (in step **(i)**) must consider these changes: the obstacle must fit inside the beam even after steering/stretching effects.

Switching between tactile feedback and levitation points

Our hybrid approach allows for the dynamic creation of both levitation traps and tactile feedback. Levitation traps can be created by overlying a signature as described in [20]. For a square array of NxN transducers, this can be easily implemented as an additional phase delay added to the one in Eq (3), producing the final phase $\psi_{lev}(i,j)$:

$$\psi_{lev}(i,j) = \begin{cases} \psi(i,j) + \pi & ,\forall i \in [0, N/2) \\ \psi(i,j) & ,\forall i \in [N/2\,, N-1) \end{cases} \quad (5)$$

Alternatively, tactile effects can be created as described in [19], by modulating the emitted signal (40kHz) at 200Hz. It must be noted that, when using this approach, all high pressure points in the field (i.e. points along the self-bending beam) will become simultaneously noticeable (unlike [12]). Coincidentally, our tests revealed that both techniques can be applied simultaneously. We successfully levitated an object on top of an obstacle while modulating the signal. This however comes at the expense of halving both the strength of the levitation trap (only active 50% of the time) and tactile points (due to the levitation signature).

EXPERIMENTAL SETUP

The following sections will describe the evaluation of our approach to implement interactive features above the passive props placed on the sound modulator. These evaluations include Finite Element Method (FEM) simulations and real measurements, using an experimental setup. We introduce both setups here and discuss the results obtained from our evaluations in the next section.

Finite Element Method Simulation

We first simulated our hybrid modulators, using a commercial FEM software (COMSOL Multiphysics 5.2a) to observe the field they would recreate. In our simulations, we set up the transmission medium as air (i.e. density 1.21 kg/m^3; speed of sound 343 m/s). The mesh elements of the models used were less than λ/8 in diameter. To simulate the properties of the real transducer array (Ultrahaptics board, version 2.0.0), we included a 16x16 array of transducers (10mm in diameter). The properties of each transducer were obtained from the manufacturer's description (muRata MA40S4S), approximating each transducer as a cylindrical piston source emitting sine-waves at 40kHz with sound pressure levels of 120dB at 30cm.

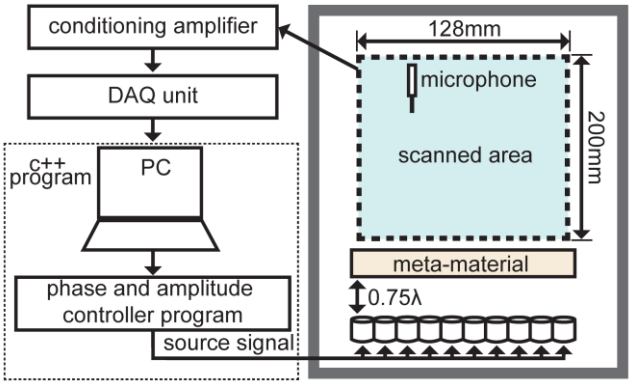

Figure 7. Schematic of our sound measurement system.

To simulate the 16 different types of discrete metamaterial bricks, we simply replicated the shape of each brick, as provided by Memoli et al. [30]. We finally fixed the metamaterial (built as combination of individual bricks) on top of the transducers' array, using a gap of 6.4mm (0.75 λ), as described in the previous section. Simulations were run in an iMac workstation (3.4 GHz Intel Core i5; 16GB DDR3 RAM; NVIDIA GeForce GTX 780M).

Sound Field Measurement System

In order to measure the actual sound fields generated, we built a custom 3D sound field scanner system (see Figure 7). We modified a commercial 3D printer (Velleman k8200), replacing its extruder by a fixed arm, holding a microphone. We then placed a PAT (Ultrahaptics board, phased controlled using Ultrahaptics SDK, ver. 2.2.1) and the metamaterial, as described in step **(iv)** earlier. We set up this measurement system, ensuring the plate is parallel to the floor and the microphone is correctly aligned to the axis of the modulator (i.e. perpendicular to the metamaterial).

Finally, we used a custom-made C++ program, delivering G-code commands to the printer to control the position of the microphone, and take samples. A delay of 0.5s was included between the displacement end and the sampling, to avoid displacement vibrations from affecting measurements. We used a B&K microphone (model 4138-A-015), a conditioning amplifier (Nexus, final gain: -20dB) and a PicoScope data acquisition unit, (Pico Instruments, model: 5444b), to capture samples and compute SPL (dB).

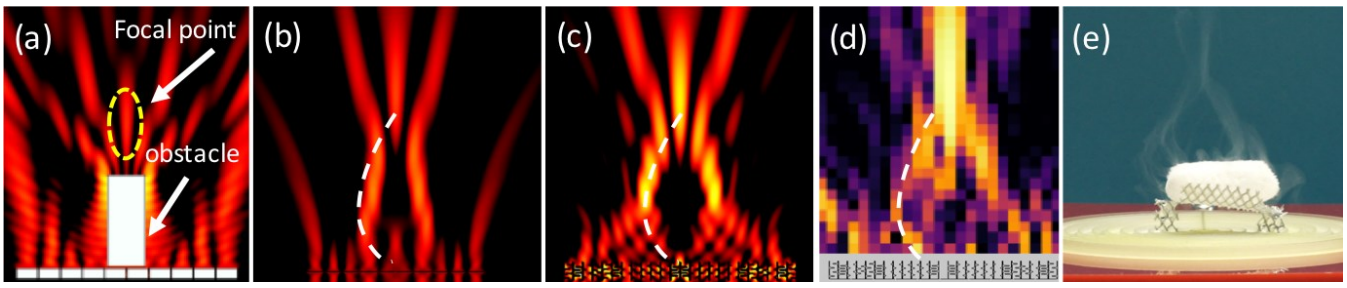

Figure 8. Sound field representation evaluating methods (a) FEM Simulation of PAT with an obstacle marked area where the control point should be (b) FEM Simulation of PAT an attempt to create a curve in (white dashed) (c) FEM Simulation of the hybrid SoundBender showing the created curve (white dashed) (d) Measurements of the SoundBender reproducing self-bending curve (e) SoundBender sound field visualization with dry ice.

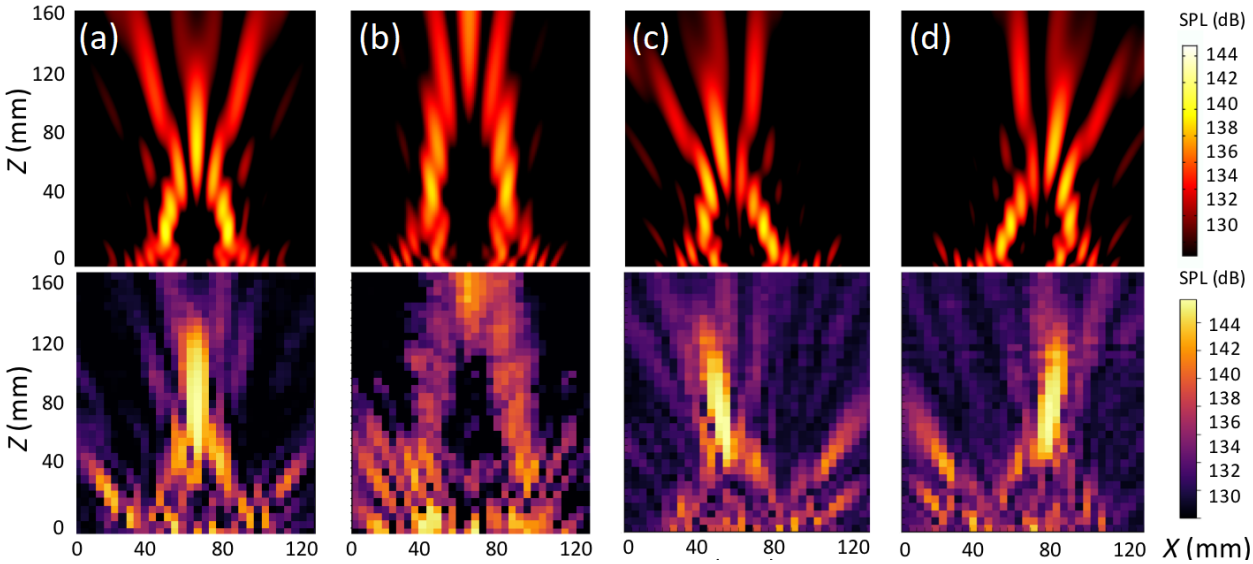

Figure 9. Evaluating our control mechanisms for extreme cases allowing levitation. Top are simulation results (COMSOL), while bottom are measurement results. (a) Static sound field generated using standing wave signal through passive metamaterial, (b) Dynamically stretched sound field (*Δz=8cm)*; (c) Shearing to left (*Δx=-2cm)*, and (d) shearing to right (*Δx=-2cm)*.

EVALUATION

We used our experimental setup to evaluate the validity of our approach in two stages. We first evaluated the feasibility of the previous approaches and SoundBender to recreate the intended sound field (i.e. the self-bending beam) at ultrasound frequencies (40kHz). We then tested the ability of our control algorithms to dynamically modify this field (i.e. stretch, steer the self-bending beam, levitate).

Self-bending Beam reconstruction

In order to test the need for our hybrid approach (and as preliminary steps in our research), we evaluated the feasibility of implementing the intended outcome (e.g. levitation/tactile feedback above a passive prop placed on top of the modulator) with simpler approaches.

Figure 8a shows a COMSOL simulation of the field resulting from creating a focal point (similar to the one in Figure 2b), in the presence of an obstacle (i.e. the passive prop). The simulation (and our tests) show that the occlusion from the prop does not allow for a high amount of acoustic pressure to be focused at the intended location.

Figure 8b illustrate our attempts to recreate self-bending beams using only a PAT, illustrating how PATs will fail to reproduce a complex field (i.e. self-bending), even without the passive prop. First, due to aliasing effects (related to PATs' lower modulator pits) cause the field created to presents low acoustic pressure along the curvature beam, being unable to levitate objects in mid-air. This confirms the predictions in [50], stating that using a PAT alone, the acoustic radiation force along the curvature beam would be insufficient to allow levitation. As a second artefact, high-pressure levels are detected inside the self-bending beam volume, where the passive prop should be located (near (0,0,0)). This would result on scattering from the object's surface and further distortion to the field generated.

Figures 8c and 8d show the sound field generated by our approach, as a FEM simulation and as directly measured by our scanner, respectively. The field generated reveals much higher acoustic pressure levels along the curve and also on top of the object. The area inside the convex hull also shows minimum acoustic pressure, effectively reducing scattering interference due to the presence of our passive prop. Finally, Figure 8e shows a visualization of the field generated, using solid CO_2 (i.e. dry ice). The vapours help identify the lines of the field, providing a quick evaluation tool to informally test different experimental conditions (e.g. implementing stretching/steering behaviours).

Similar situations to 8a (field in the presence of the prop) were also simulated for a PAT and for SoundBender, and can be found in supplementary material. Although removed here for brevity, they further illustrate the need for hybrid modulators to create complex (e.g. self-bending) fields, and enable the dynamic behaviours explored in our applications.

Dynamic control of the self-bending beam

We tested the ability of our setup to dynamically adjust the shape of the static field encoded in the metamaterial. We created a levitation trap on top of an obstacle, and tested its performance at various stretching values (i.e. displacement in Z) from Figure 9a to 9b and steering values as in Figure 9c and 9d (i.e. displacements in XY plane). We found that our arrangement allowed for maximum displacements in X and Y axes of ≈ 2cm and up to 8cm along the Z axis. These extreme scenarios are illustrated in Figure 9, showing the results from our FEM simulations (upper row) and actual measurements of the field (bottom).

The possibility to create tactile feedback was also empirically tested, by modulating our carrier wave (40kHz) with an envelope at 200Hz (i.e. within skin receptor's response). This resulted in a force of 2.3mN behind the

Figure 10. We explore applications controlling three types of interactive features: (a) Haptic feedback behind an obstacle; (b) Levitation around the obstacle; (c) manipulation of non-solid objects, changing the fire's angle.

obstacle, perceivable to over 90% of the users according to related studies [48,49]. Our tests also revealed that the tactile sensation is still vivid in ≈3cm displacement in x and y-axes and ≈10cm in z axis. It is also worth noting that even if the tactile feedback is most perceivable above the object, the space around it (i.e. along the self-bending beam) al so produces tactile feedback. This allows for feedback along the continuous surface created by our self-bending beam.

EXAMPLE APPLICATIONS

In this section, we explore some of the applications enabled by our approach, using our example self-bending beam. This provides a way to create dynamic control points beyond occluding objects. Our exploration is structured around the three basic types of interactive features that can be dynamically controlled with our approach: a) modulated high pressure points (i.e. tactile feedback); b) levitated objects; and c) non-solid elements. We also restrict this exploration to small form factors (as demonstrated in the paper), but also, to formats that allow the free placement (or removal) of passive props/obstacles on top of SoundBender.

Around Object tactile feedback

Figure 10a shows a basic example modulating the self-bending beam at 200Hz, to create a tactile field. Such field will show maximum radiation pressure above the object, but also high pressure along the whole surface of the curve (i.e. around the sides of the object). The presence of tactile feedback before actually touching the object (on top and/or around it) can be used to provide users with a *feed-forward*, informing them of the outcome of their actions before starting the interaction with the tangible passive prop. The dynamic adjustment of the feedback provided can enrich the granularity of the contextual information delivered. For instance, changing the modulating frequency can produce different tactile sensations, each with a particular meaning. Moving the beam (i.e. steer/stretch) can guide users hand towards the object, facilitating eyes-free interactions.

Around object levitated objects

The combination of replaceable props and levitated objects on top of these props (as seen in Figure 10b), easily lends itself to the creation of interactive decorative elements, interactive visualizations and toys of different types. For instance, in the context of a board game, passive props can be used to represent various characters/creatures, while the levitated elements can be used to represent spells/power ups affecting it. The speed or trajectory of the levitated bead can indicate the current status of the power up, letting it fall as its effect finishes. Additional sensors (e.g a proximity sensor) on the passive prop could let the prop react to the levitated element (e.g. illuminate the eyes, detect active power-up), extending interactivity to the passive prop also. The need to manually place the levitated objects would add an element of skill and uncertainty to the game (i.e. a player can fail to summon a power-up, if the object falls). In a learning environment (e.g. museum), combining different props and levitated beads (e.g. coloured differently) could lead to exploratory interactions, to learn different aspects about the prop object. For instance, placing a green bead on top of a country, could reveal the percentage of its surface covered by forests. A black bead could reveal its carbon footprint, while dynamically changing the height of the bead could reveal its evolution over time. Other materials (e.g. food, liquid) have been used for levitation before [5][8][9] and could also be applicable to SoundBender.

Around object non-solid features

Pressure fields from our modulator can also affect non-solid elements, such as the fire from a candle (see Figure 10c), or aerosols, like the dry ice used in Figure 8e. This could extend on the range of animated elements that can be added on top of the passive prop. In the first case, the direction of the flame in Figure 10c aligns to the steering direction of the sound field, while the intensity of the flame is affected by the intensity of the field (i.e. brighter at lower pressures). For instance, in the case of a cupcake with a lit candle on it, the direction of the flame could be synchronized to an external source (e.g. a happy birthday song). Using a scented source instead (e.g. incense), could be used to implement smell delivery devices, with SoundBender controlling the direction of the flow. Such flow control could provide non-solid displays with additional approaches to control the trajectory of the diffuser, which is acknowledged as one of the aspects constraining the format where such non-solid diffusers can be applied [51].

LIMITATIONS AND DISCUSSION

This paper represents an effort to draw techniques from related fields (acoustics, optics) into a reproducible approach. This will allow HCI practitioners to use hybrid sound modulators to explore high resolution sound fields which are simply not reproducible using PATs only.

This however, does not imply an absolute superiority of hybrid modulators vs PATs. PATs provide a great versatility, while hybrid modulators (like SoundBender) will only be useful in scenarios where a sound field with high spatial resolution is needed, but only smaller dynamic changes are required. Even so, the spatial configuration of the modulator (i.e. its shape, spatial arrangement) will be just as relevant as the type of modulator itself. For instance, either a flat PAT or SoundBender will struggle to recreate a standing wave pattern, while this is trivial, with simply two transducers. Thus, any type of modulator must simply be considered as a tool, with its strengths and limitations. We thus believe that our hybrid modulators provide a tool for the HCI community to explore new applications tapping on more complex sound fields, with our method helping designers to identify/address the main challenges and pitfalls related to the use of these hybrid modulators.

Our exploration has been focused on self-bending beams. This helped us to explore many practical aspects related to the creation of hybrid modulators. The two most important ones were: i) the higher relevance of the modulator pitch vs their phase or amplitude; and ii) the feasibility to delegate dynamic phase and amplitude control to the PAT, even if this only allows lower spatial resolution on the sound field.

Our exploration with self-bending beams has been however limited to phase control, which rules the geometry of the sound field. Control of the amplitude (using the PAT) could enable other effects. For instance, the injective mapping in Figure 3b identifies the points on the hybrid modulator that contribute to the intensity of each part of the curve. Dynamically adjusting the amplitude of transducers contributing to specific parts of the curve (the part they are "tangent" to) could provide more control/dynamic effects. For instance, reinforcing a section of the curve could create a "ring like" field. Quickly moving intensity along the curve (e.g. from the top of the beam downwards) could create a tactile feedback similar to pressing a button.

Our exploration of the influence of the gap between the metamaterial and the PAT also revealed a smoothing effect on the phases used on the PAT. This limits the kind of dynamic effects that the PAT can create, indicating that such operations must avoid high frequency changes. This must be considered when exploring new algorithms for dynamic control of this kind of hybrid modulators. Other aspects, such as the phase distribution across this gap, or even the use of coupling layers between the metamaterial and the PAT should be explored for further control.

It is also worth noting that, although we could apply levitation signatures successfully, other levitation signatures (e.g. bottle beams [20]) resulted in high pressure inside the self-bending volume. This kind of levitation was still possible without obstacles, but obstacle objects resulted on scattering from the obstacle object.

Our method can also be applied to sound fields other than self-bending beams, opening a space for further exploration. For instance, metamaterials could be used to encode specific tactile patterns (e.g. a multipoint pattern, representing a tactile "icon"). The designer could then focus on creating different modulation schemes (e.g. not only the usual modulation at 200Hz, with 50% duty cycle [19]), to test various tactile experiences.

Replacing the metamaterial with another one (i.e. encoding a different location of the points/ tactile "icon") could help explore tactile stimuli quickly. This could also allow interactive scenarios beyond those explored in the paper, with the user replacing either the metamaterial, the passive prop or the levitated beads to achieve different effects. This could encourage new ways of thinking about tangible user interfaces, with metamaterials, obstacles and levitated objects working as modifiers for the tangible element.

CONCLUSION

This paper presented SoundBender, a hybrid sound modulator combining acoustic metamaterials and phased arrays of transducers (PATs). The metamaterial is used to encode complex sound fields that cannot be created using PATs alone. The PAT allows a dynamic and real-time control of the sound field.

We illustrated this approach using self-bending beams, which allows for interactive artefacts featuring passive props located on top of the modulator and interactive elements (i.e. tactile points, levitated matter and non-solid features) above the prop.

We described a five-step method to guiding the creation of such interactive artefacts, starting from the basic shape of the passive prop, and detailing the fabrication of the hybrid sound modulator and the control algorithms to enable interactive features above/around the prop.

We demonstrated the feasibility of our approach, and compared it against alternative approaches (focused points and self-bending beams implemented with a single phased array). We also demonstrated dynamic control of the interactive features (tactile points and levitated object). In the end of the paper we provided an overview of the potential applications of the SoundBender to produce novel interactive experiences but also, to enable the HCI community to draw on our approach and explore even further the dynamical control capabilities of alternative complex sound fields.

ACKNOWLEDGMENTS

This project was funded by the European Union's Horizon 2020 research and innovation programme under the FET-Open Scheme with grant agreement No 737087 and Universiti Teknikal Malaysia Melaka (UTeM) and Ministry of Higher Education, Malaysia (MoHE). We thank Luis Veloso for taking the images and videos

REFERENCES

1. Ivan. E. Sutherland. 1965. The ultimate display. In *Proc. Congr. Int. Fed. Inf. Process*, pp. 506–508.
2. Hiroshi Ishii, Dávid Lakatos, Leonardo Bonanni and Jean-B. Labrune. 2012. Radical Atoms: Beyond Tangible Bits, Toward Transformable Materials. *Interactions*. vol. XIX, no. February, pp. 38–51. http://doi.acm.org/10.1145/2065327.2065337
3. Tobias Alrøe, Jonas Grann, Erik Grönvall, Marianne G. Petersen and Jesper L. Rasmussen. 2012. Aerial Tunes: Exploring Interaction Qualities of Mid-air Displays. In *Proc. 7th Nord. Conf. Human-Computer Interact. Mak. Sense Through Des.*, pp. 514–523. http://doi.acm.org/10.1145/2399016.2399095
4. Jinha Lee, Rehmi Post, and Hiroshi Ishii. 2011. ZeroN: Mid-Air Tangible Interaction Enabled by Computer Controlled Magnetic Levitation. In *Proceedings of the 24th Annual ACM Symposium on User Interface Software and Technology* (UIST '11), pp. 327–366. http://doi.acm.org/10.1145/2047196.2047239
5. Yoichi Ochiai, Takayuki Hoshi and Jun Rekimoto. 2014. Pixie Dust : Graphics Generated by Levitated and Animated Objects. In *ACM Trans. Graph.*, vol. 33, no. 4, p. Article 85. http://doi.acm.org/10.1145/2601097.2601118
6. Themis Omirou, Asier Marzo, Sue A. Seah and Sriram Subramanian. 2015. LeviPath: Modular Acoustic Levitation for 3D Path Visualisations. In *Proceedings of the ACM Conference on Human Factors in Computing Systems* (CHI'15*)*, vol. 1, pp. 309–312. http://dx.doi.org/10.1145/2702123.2702333
7. Asier Marzo. 2016. GauntLev: A Wearable to Manipulate Free-floating Objects. In *Proceedings of the 2016 CHI Conference on Human Factors in Computing Systems* (CHI'16*)*, pp. 3277–3281. http://doi.acm.org/10.1145/2858036.2858370
8. Daniele Foresti, Majid Nabavi, Mirko Klingauf, Aldo Ferrari and Dimos Poulikakos. 2013. Acoustophoretic contactless transport and handling of matter in air. In *Proceedings of the National Academy of Sciences* (PNAS), vol. 110, no. 31, pp. 12549–12554. https://doi.org/10.1073/pnas.1301860110
9. Chi T. Vi, Asier Marzo, Damien Ablart, Gianluca Memoli, Sriram Subramanian, Bruce Drinkwater and Marianna Obrist. 2017. TastyFloats : A Contactless Food Delivery System. In *Proc. 2017 ACM Int. Conf. Interact. Surfaces Spaces* (ISS'17), pp. 161–170. https://doi.org/10.1145/3132272.3134123
10. Deepak R. Sahoo, Takuto Nakamura, Asier Marzo, Themis Omirou, Michihiro Asakawa and Sriram Subramanian. 2016. JOLED: A Mid-air Display based on Electrostatic Rotation of Levitated Janus Objects. In *Proceedings of the 29th ACM Symposium on User Interface Software and Technology* (UIST '16), pp. 437–448. http://dx.doi.org/10.1145/2984511.2984549
11. Julie R. Williamson, Euan Freeman and Stephen Brewster. 2017. Levitate: Interaction with floating particle displays. In *Proceeding of the 6th ACM International Symposium on Pervasive Displays* (PerDis 2017). http://dx.doi.org/10.1145/3078810.3084347
12. Benjamin Long, Sue A. Seah, Tom Carter and Sriram Subramanian. 2014. Rendering volumetric haptic shapes in mid-air using ultrasound. In *ACM Transaction on Graphics,* vol. 33, no. 6, pp. 1–10. http://doi.acm.org/10.1145/2661229.2661257
13. William H. Press, Saul A. Teukolsky, William T. Vetterling and Brian P. Flannery. *1987. Numerical Recipes: The Art of Scientific Computing*, vol.29, no.4.
14. Alexandra Ion, Ludwig Wall, Robert Kovacs and Patrick Baudisch. 2017. Digital Mechanical Metamaterials. In *Proceedings of the ACM Conference on Human Factors in Computing Systems* (CHI'17*)*, pp. 977–988. http://dx.doi.org/10.1145/3025453.3025624
15. Laura Ferrarello and Kevin Walker. 2016. The form of sound through hybrid materials. In *ACM SIGGRAPH 2016,* pp. 1–2. http://dx.doi.org/10.1145/2945078.2945165
16. Dingzeyu Li, David I.W. Levin, Wojciech Matusik, and Changxi Zheng. 2016. Acoustic voxels. In *ACM Transaction on Graphics*, vol. 35, no. 4, pp. 1–12. http://dx.doi.org/10.1145/2897824.2925960
17. J. H. Thomson and J. J. Poynting. 1900. *A text Book of Physics: Sound.* Charles Griffin & Co.
18. E. H. Brandt. 2001. Suspended by sound. In *Nature*, vol. 413, no. October, pp. 474–475. http://doi.org/10.1038/35097192.
19. Tom Carter, Sue A. Seah, Benjamin Long, Bruce Drinkwater and Sriram Subramanian. 2013. UltraHaptics. In *Proceedings of the 26th Annual ACM Symposium on User Interface Software and Technology* (UIST '13*)*, pp. 505–514. http://dx.doi.org/10.1145/2501988.2502018

20. Asier Marzo, Sue A. Seah, Bruce W. Drinkwater, Deepak R. Sahoo, Benjamin Long, and Sriram Subramanian. 2015. Holographic acoustic elements for manipulation of levitated objects. In *Nature Communications*, vol. 6, no. May, pp. 1–7. http://dx.doi.org/10.1038/ncomms9661

21. Themis Omirou, Asier M. Perez, Sriram Subramanian and Anne Roudaut. 2016. Floating Charts: Data Plotting using Free-Floating Acoustically Levitated Representations. In *IEEE Symposium on 3D User Interfaces* (3DUI), pp. 187–190. https://doi.org/10.1109/3DUI.2016.7460051

22. A. Marzo, A. Ghobrial, L. Cox, M. Caleap, A. Croxford, and B. W. Drinkwater. 2017. Realization of compact tractor beams using acoustic delay-lines. In *Applied. Physics Letters*, vol. 110, no. 1, pp. 1–6. http://dx.doi.org/10.1063/1.4972407

23. J. W. Waanders. 1991. *Piezoelectric Ceramics: Properties and Apps* (6th ed.), Philips Components.

24. Murata Ultrasonic Sensor. 2008. *Ultrasonic Sensor*. Murata Manufacturing Co., Ltd., pp. 1–17.

25. Wenqi Wang, Yangbo Xie, Bogdan-I. Popa and Steven A. Cummer. 2016. Subwavelength diffractive acoustics and wavefront manipulation with a reflective acoustic metasurface. In *Journal of Applied Physics*, vol. 120, no. 19. http://dx.doi.org/10.1063/1.4967738

26. Yong Li, Xue Jiang, Rui-q. Li, Bin Liang, Xin-y. Zou, Lei-l. Yin and Jian-c. Cheng. 2014. Experimental realization of full control of reflected waves with subwavelength acoustic metasurfaces. In *Physical Review Applied,* vol. 2, no. 6, pp. 1–11. https://doi.org/10.1103/PhysRevApplied.2.064002

27. Kai Melde, Andrew G. Mark, Tian Qiu and Peer Fischer. 2016. Holograms for acoustics. In *Nature Letter*, vol. 537, no. 7621, pp. 518–522. http://doi.org/10.1038/nature19755

28. Yangbo Xie, Chen Shen, Wenqi Wang, Junfei Li, Dingjie Suo, Bogdan I. Popa, Yun Jing and Steven A. Cummer. 2016. Acoustic Holographic Rendering with Two-dimensional Metamaterial-based Passive Phased Array. In *Scientific Reports*, vol. 6, no. July, pp. 1–6. http://doi.org/10.1038/srep35437

29. Andrea Colombi, Daniel Colquitt, Philippe Roux, Sebastien Guenneau and Richard V. Craster. 2016. A seismic metamaterial: The resonant metawedge. In *Scientific Reports*, vol. 6, no. 1, p. 27717. http://doi.org/10.1038/srep27717

30. Gianluca Memoli, Mihai Caleap, Michihiro Asakawa, Deepak R. Sahoo, Bruce W. Drinkwater, and Sriram Subramanian. 2017. Metamaterial bricks and quantization of meta-surfaces. In *Nature Communications*, vol. 8, pp. 1–8. http://doi.org/10.1038/ncomms14608

31. Xing Chen, Xianchen Xu, Shigang Ai, HaoSen Chen, Yongmao Pei, and Xiaoming Zhou. 2014. Active acoustic metamaterials with tunable effective mass density by gradient magnetic fields. In *Applied Physics Letters*, vol. 105, no. 7. http://dx.doi.org/10.1063/1.4893921

32. Bogdan-I. Popa, Durvesh Shinde, Adam Konneker, and Steven A. Cummer. 2015. Active acoustic metamaterials reconfigurable in real time. In *Physical Review B,* vol. 91, no. 22, pp. 1–5. https://doi.org/10.1103/PhysRevB.91.220303

33. Giuseppe Pesce, Giorgio Volpe, Onofrio M. Marago, Philip H. Jones, Sylvain Gigan, Antonio Sasso and Giovanni Volpe. 2015. A Step-by-step Guide to the Realisation of Advanced Optical Tweezers. In *Journal of the Optical Society of America B*, vol. 32, no. 5, pp. 84–98, 2015. http://dx.doi.org/10.1364/JOSAB.32.000B84

34. P. S. Salter, Z. Iqbal, and M. J. Booth. 2013. Analysis of the Three-Dimensional Focal Positioning Capability of Adaptive Optic Elements. In *International Journal of Optomechatronics*, vol. 7, no. 1, pp. 1–14. http://dx.doi.org/10.1080/15599612.2012.758791

35. Martin Maldovan. 2013. Sound and heat revolutions in phononics. In *Nature*, vol. 503, no. 7475, pp. 209–17. http://doi.org/10.1038/nature12608

36. Yong Li and M. B. Assouar. 2015. Three-dimensional collimated self-accelerating beam through acoustic metascreen. In *Scientific Reports*, vol. 5, no. 1, p. 17612. http://dx.doi.org/10.1038/srep17612

37. He Gao, Zhong-m. Gu, Bin Liang, Xin-y. Zou, Jing Yang, Jun Yang, and Jian-c. Cheng. 2016. Acoustic focusing by symmetrical self-bending beams with phase modulations. In *Applied Physics Letters*, vol. 108, no. 7. http://dx.doi.org/10.1063/1.4941992

38. Fan Zheng, Ying Li, Hsiu-S. Hsu, Changgeng Liu, Chi T. Chiu, Changyang Lee, Hyung H. Kim, and K. Kirk Shung. 2012. Acoustic trapping with a high frequency linear phased array. *Applied Physics Letters*, vol. 101, no. 21, 2012. http://dx.doi.org/10.1063/1.4766912

39. Jungwoo Lee, Shia-Y. Teh, Abraham Lee and Hyung H. Kim, Changyang Lee, and K. Kirk Shung. 2009. Single beam acoustic trapping. In *Applied Physics Letters*, vol. 95, no. 7. http://dx.doi.org/10.1063/1.3206910

40. Ying Li, Changyang Lee, Ruimin Chen, Qifa Zhou, and K. Kirk Shung. 2014. A feasibility study of in vivo applications of single beam acoustic tweezers. In *Applied Physics Letters*, vol. 105, no. 17. http://dx.doi.org/10.1063/1.4900716

41. Peng Zhang, Tongcang Li, Jie Zhu, Xuefeng Zhu, Sui Yang, Yuan Wang, Xiaobo Yin and Xiang Zhan. *2014.* Generation of acoustic self-bending and bottle beams by phase engineering. In *Nature Communications*, vol. 5, pp. 1–9. http://doi.org/10.1038/ncomms5316

42. S. Zhao, Y. Hu, J. Lu, X. Qiu, J. Cheng, and I. Burnett. 2014. Delivering Sound Energy along an Arbitrary Convex Trajectory. In *Scientific Reports*, vol. 4, no. 6628, pp. 1–6. http://doi.org/10.1038/srep06628

43. Georgios A. Siviloglou and Demetrios N. Christodoulides. 2007. Accelerating finite energy Airy beams. In *Optics Letters*, vol. 32, no. 8, p. 979-981. http://doi.org/10.1364/OL.32.000979

44. Elad Greenfield, Mordechai Segev, Wiktor Walasik and Oren Raz. 2011. Accelerating light beams along arbitrary convex trajectories. In *Physical Review Letters*, vol. 106, no. 21, pp. 1–4. http://doi.org/10.1103/PhysRevLett.106.213902

45. Mohd A. Norasikin, Gianluca Memoli, Diego M. Plasencia and Sriram Subramanian. 2017. Acoustic Levitation By a Metamaterial-Based Cloak. In *24th International Congress on Sound and Vibration* (ICSV'24), pp.1–8.

46. Edwin Catmull and Raphael Rom. 1974. A Class of Local Interpolating Splines. In *Computer Aided Geometric Design*, pp. 317–326. http://doi.org/10.1016/B978-0-12-079050-0.50020-5

47. Naohisa Okada, Tomoyoshi Shimobaba, Yasuyuki Ichihashi, Ryutaro Oi, Kenji Yamamoto, Minoru Oikawa,Takashi Kakue, Nobuyuki Masuda, and Tomoyoshi Ito. 2013. Band-limited double-step Fresnel diffraction and its application to computer-generated holograms. In Optics. Express, vol. 21, no. 7, p. 9192. http://doi.org/10.1364/OE.21.009192

48. Yoichi Ochiai, Kota Kumagai, Takayuki Hoshi, Satoshi Hasegawa and Yoshio Hayasaki. 2016. Cross-Field Aerial Haptics : Rendering Haptic Feedback in Air with Light and Acoustic Fields. In *Proceedings of the ACM Conference on Human Factors in Computing Systems* (CHI'16*)*, pp. 3238–3247. http://dx.doi.org/10.1145/2858036.2858489

49. Georgios Korres and Mohamad Eid. 2016. Haptogram: Ultrasonic Point-Cloud Tactile Stimulation. In *IEEE Access*, vol. 4, pp. 7758–7769. https://doi.org/10.1109/ACCESS.2016.2608835

50. P. J. Westervelt. 1951. The Theory of Steady Forces Caused by Sound Waves. *The Journal of the Acoustical Society of America*, vol. 23, no. 3, pp. 312–315. http://dx.doi.org/10.1121/1.1906764

51. Deepak R. Sahoo, Diego M. Plasencia, and Sriram Subramanian. 2015. Control of Non-Solid Diffusers by Electrostatic Charging. In *Proceedings of the 33rd Annual ACM Conference on Human Factors in Computing Systems* (CHI'15), 2015, vol. 1, pp. 11–14. http://dx.doi.org/10.1145/2702123.2702363